Analyst

Accepted Manuscript

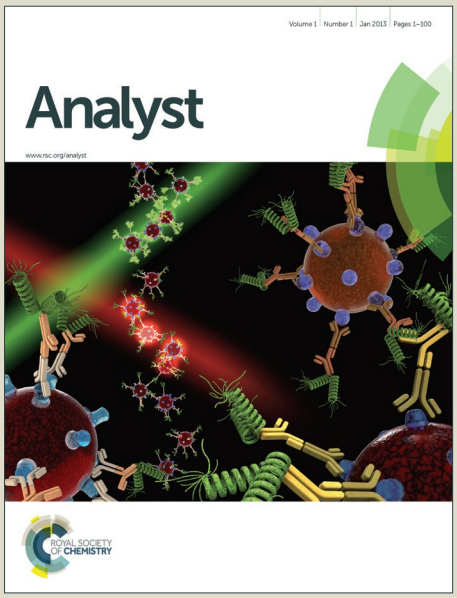

ROYAL SOCIETY OF CHEMISTRY

www.rsc.org/analyst

View Article Online
DOI: 10.1039/C4AN01788A

A Comparative Study of Graphene-Hydrogel Hybrid Bionanocomposites for Biosensing

Burrs, S.L.[1], D.C. Vanegas[1, 2], M. Bhargava[1], N. Mechulan[1] P. Hendershot[3], H. Yamaguchi[3], C. Gomes[4], and E.S. McLamore[1*]

[1]*Agricultural & Biological Engineering Department, University of Florida, 1741 Museum Road, Gainesville, FL, USA*

[2]*Department of Food Engineering, Universidad del Valle, Ciudad Universitaria Meléndez, Edif. 338, Cali, Colombia*

[3]*Department of Mechanical and Aerospace Engineering, University of Florida, 226 MAE-B Building, Gainesville, FL, USA*

[4]*Department of Biological & Agricultural Engineering, Texas A&M University, 201 Scoates Hall College Station, TX, USA*

[*]*Email: emclamor@ufl.edu Tel: +1 352 392 1864*

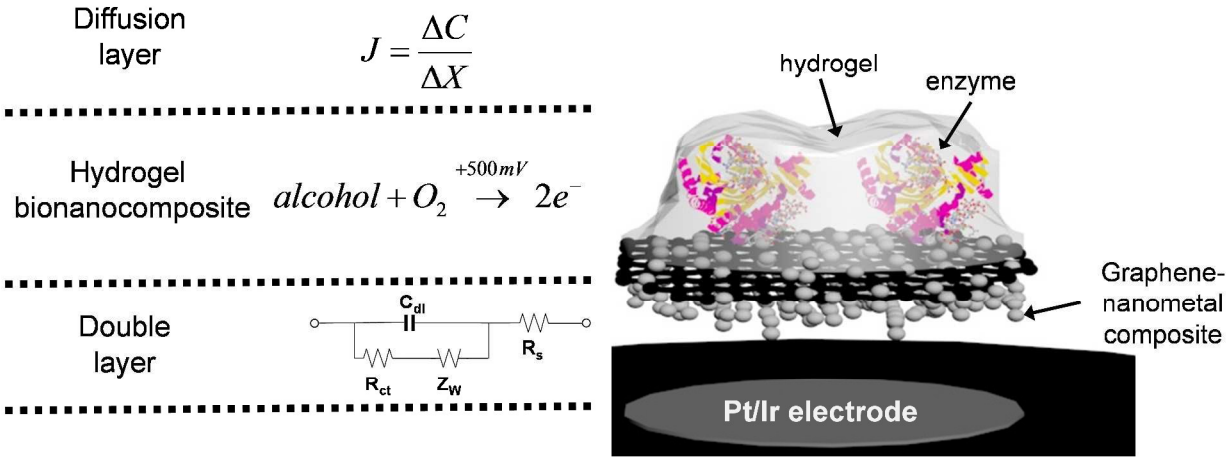

Graphical abstract. This study compares the performance of four different hydrogels used as protein encapsulants in a graphene-nanometal-enzyme biosensor using alcohol oxidase as the biorecognition element. Hydrogels composed of chitosan, poly-*N*-isopropylacrylamide, silk fibroin, and cellulose nanocrystals were compared in terms of electroactive surface area, electron transfer kinetics, film morphology, sensitivity, response time, limit of detection, hysteresis, and shelf life.

View Article Online
DOI: 10.1039/C4AN01788A

Abstract

Hydrogels have become increasingly popular as immobilization materials for cells, enzymes and proteins for biosensing applications. Enzymatic biosensors that utilize hydrogel as an encapsulant have shown improvements over other immobilization techniques such as cross linking and covalent bonding. However, to date there are no studies which directly compare multiple hydrogel-graphene nanocomposites using the same enzyme and test conditions. This study compares the performance of four different hydrogels used as protein encapsulants in a mediator-free biosensor based on graphene-nanometal-enzyme composites. Alcohol oxidase (AOx) was encapsulated chitosan, poly-*N*-isopropylacrylamide (PNIPAAM), silk fibroin or cellulose nanocrystals (CNC) hydrogels, and then spin coated onto a nanoplatinum-graphene modified electrode. The transduction mechanism for the biosensor was based on AOx-catalyzed oxidation of methanol to produce hydrogen peroxide. To isolate the effect(s) of stimulus response on biosensor behavior, all experiments were conducted at 25 °C and pH 7.10. Electroactive surface area (ESA), electrochemical impedance spectroscopy (EIS), sensitivity to methanol, response time, limit of detection, and shelf life were measured for each bionanocomposite. Chitosan and PNIPAAM had the highest sensitivity (0.46 ± 0.2 and 0.3 ± 0.1 μA mM^{-1}, respectively) and electroactive surface area (0.2 ± 0.06 and 0.2 ± 0.02 cm^2, respectively), as well as the fastest response time (4.3 ± 0.8 and 4.8 ± 1.1 s, respectively). Silk and CNC demonstrated lower sensitivity (0.09 ± 0.02 and 0.15 ± 0.03 μA mM^{-1}, respectively), lower electroactive surface area (0.12 ± 0.02 and 0.09 ± 0.03 cm^2, respectively), and longer response time (8.9 ± 2.1 and 6.3 ± 0.8 s, respectively). The high porosity of chitosan, PNIPAAM, and silk gels led to excellent transport, which was significantly better than CNC bionanocomposites. Electrochemical performance of CNC bionanocomposites were relatively poor, which may be linked to poor gel stability. The differences between the Chitosan/PNIPAAM group and the Silk/CNC group were statistically significant ($p < 0.05$) based on ANOVA. Each of these composites was within the range of other published devices in the literature, while some attributes were significantly improved (namely response time and shelf life). The main advantages of these hydrogel composites over other devices is that the only one enzyme is required, all materials are non-toxic, the sensor does not require mediators/cofactors, and the shelf life and response time are significantly improved over other devices.

Keywords: hydrogel, graphene, nanocomposite, alcohol oxidase,

Introduction

Hydrogels demonstrate characteristics that are promising for enzyme encapsulation in biosensing, such as water absorption, swelling, cross linking, resistance to dissolution, and formation of hydrophilic aqueous microenvironments (Jang 2010). Furthermore, many natural and synthetic hydrogels are biocompatible, abundant materials that meet requirements for high performance biosensors based on sustainable materials. Hydrogels can significantly improve enzyme activity in thin films, which is the most critical factor in the performance of enzymatic biosensors (Buenger et. al., 2012). Four hydrogels that have recently gained much attention in the development of biosensors include chitosan, poly-*N*-isopropylacrylamide (PNIPAAM), silk fibroin, and cellulose nanocrystals (CNC) (Zhai, 2013). These

View Article Online
DOI: 10.1039/C4AN01788A

hydrogels have chemical, physical, and electrical properties that are useful in enzymatic biosensing, particularly when proteins such as oxidoreductase are used as the biorecognition agent.

Chitosan is a biocompatible, nontoxic, inert, and hydrophilic natural biopolymer derived from crustacean shells (from chitin) (López-León et al., 2005). The amino groups in chitosan facilitate enzyme immobilization via ionic bonding between carboxyl groups on the protein surface and the hydrogel (Miao and Tan et al., 2000; Suginta 2013; Pauliukaite et al., 2010). PNIPAAM is a polymer that is synthesized by free radical polymerization of isopropylacrylamide monomers (Ahmed 2013). PNIPAAM contains both hydrophilic groups (acylamino group, – CONH) and hydrophobic groups (isopropyl, $–CH(CH_3)_2$) , both of which are known to form hydrogen bonds with proteins. Silk fibers (composed of the proteins sericin and fibroin) are the strongest, toughest natural fibers known. Silk-based materials have been used for optics, photonics, and electronics (Tao et al., 2012; Liu et al., 1996; Kim et al., 2004, Rockwood et al., 2011; Lee et al., 2005). Hydrogels composed of silk fibroin have been used for immobilization of proteins by hydrogen bonding within the beta pleated fibroin sheets (Hu et al., 2005). CNC are formed when cellulose fibers are subjected to acid hydrolysis, and the fibers yield defect-free, rod-like crystalline residues (Reiner and Rudie, 2013). CNC has a high surface area, low density, and high mechanical strength; in addition, it is a renewable, sustainable and abundant material (Habibi et al., 2009). Many enzymes (including alcohol oxidase) are known to have carbohydrate binding modules (CBM) that form covalent bonds with cellulose (Levasseur et al., 2013). Chitosan, PNIPAAM, and CNC are known to exhibit stimulus-response behavior, resulting in significant structural changes with slight changes in pH and/or temperature (Zhang et al., 2000; Dufresne, 2010; Francisco et al., 2011). On the other hand, silk hydrogels do not behave as a stimulus-responsive material due to the presence of crystals that ensure dimensional stability over a wide temperature range, although acidic conditions have been shown to induce swelling in a few studies (Gil et al., 2005, Hu et al., 2010).

The state of the art in electrochemical biosensing is to immobilize enzymes on electrodes modified with a transducer nanomaterial such as nanometals, nanocarbon, or other conductive nanomaterials (Shao et al., 2010; He et al., 2011; Kim and Palmore, 2012; Kotanen et al., 2013). This approach is useful because materials such as graphene-platinum nanocomposites have demonstrated enhanced sensitivity and response time (Vanegas et al., 2014; Chaturvedi et al., 2014). When hydrogels are combined with conductive nanomaterials, a highly porous, hydrophillic network is formed that is capable of encapsulating enzymes with high electron mobility (Yuan et. al., 2013, Bai et. al., 2011, Pauliukaite et. al., 2010).

This manuscript compares the use of chitosan, PNIPAAM, silk fibroin and CNC hydrogels for immobilization of alcohol oxidase (AOx) on a graphene-platinum nanocomposite (Figure 1). AOx is useful in the measurement of short chain alcohols in the pulp processing, food/beverage, bioprocessing, clinical, and forensic industries (Akin et al., 2011, Das et al., 2013, Wu et al., 2007, Jang et al. 2010). A wide variety of materials have been investigated for encapsulating AOx, including nitrocellulose (Boujtita et al., 2000), polyvinyl ferrocenium (Gulce et al., 2002), graphite-doped Teflon (de Prada et al., 2003), electropolymerised dihydroxynaphthalene (Badea et al., 2003), polyvinyl imidazole (Alpeeva et al., 2005), Teflon (Akyilmaz and Dinckaya, 2005), polypyrrole (Carelli et al., 2006), chitosan/eggshell membrane (Wen et al., 2007), polyamidoamine dendrimers (Akin et al., 2010), polyethyleneimine (Das et al., 2013) and polycarbonyl sulfonate (Alpeeva et al., 2001). However, to date there are no comparative studies which directly address how different hydrogels interact with the same graphene-nanometal

View Article Online
DOI: 10.1039/C4AN01788A

transducer layer in biosensing with AOx. This study shows that hydrogels are an excellent material for encapsulating AOx on graphene-nanometal hybrid composites. The sensors showed increased shelf life and response time, while sensitivity and range were within the range of other sensors in the published literature.

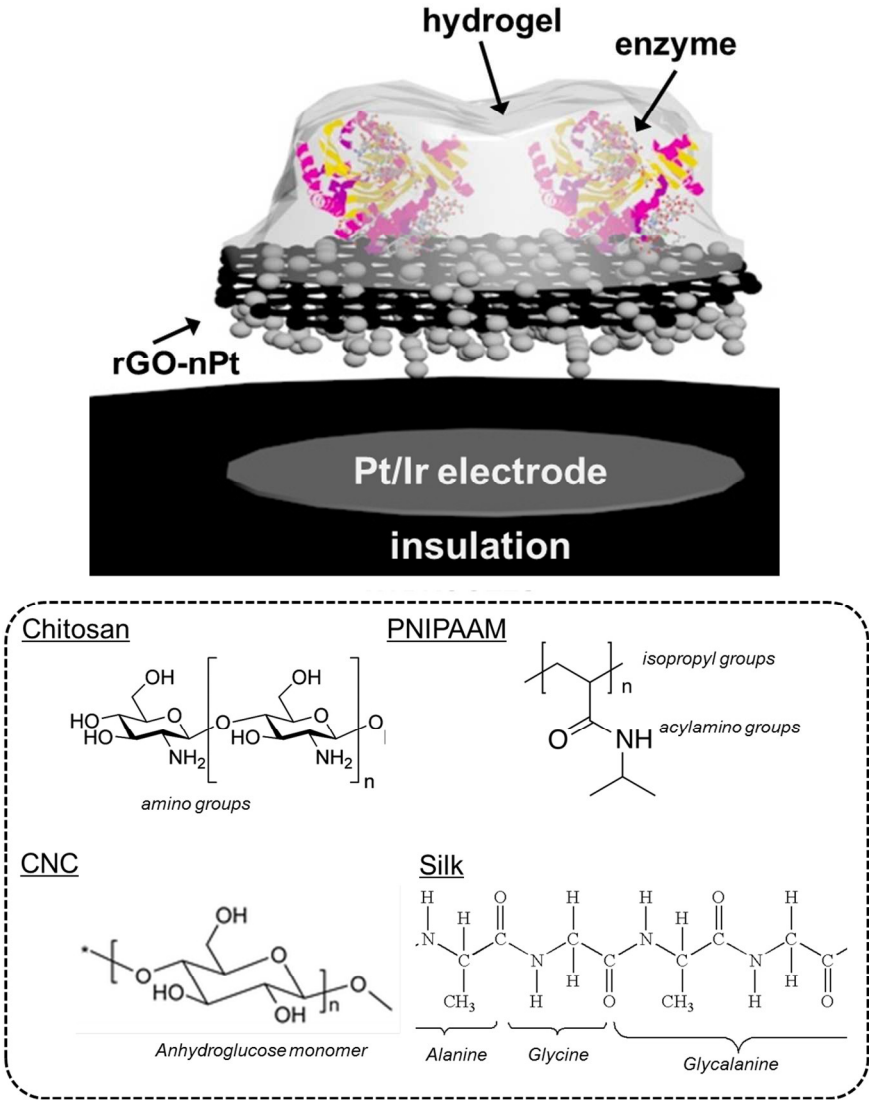

Figure 1. This manuscript presents a comparative study of hydrogel-graphene hybrid nanocomposites for biosensing using AOx to measure short chain alcohols. Hydrogels analyzed include chitosan, PNIPAAM, silk fibroin, and CNC. AOx forms ionic bonds with amino groups found in chitosan hydrogels. AOx is encapsulated in PNIPAAM by hydrogen bonding with acylamino and isopropyl groups. AOx binds to CNC via carbohydrate binding modules. Silk-based hydrogels encapsulate AOx through hydrogen bonding within beta pleated sheets of the structural fibroin.

View Article Online
DOI: 10.1039/C4AN01788A

Experimental

Materials and Reagents

Single-layered graphene oxide (GO) was purchased from ACS Material (Medford, MA). Lead acetate (30% *w/v*), chloroplatinic acid (8% *w/w*), chitosan (M_w 190-310 kDa, 75-85% deacetylated chitin) and alcohol oxidase (type AOX1) from the methylotrophic yeast *Pichia pastoris* (M_W = 975 kDa) were purchased from Sigma-Aldrich (St Louis, MO). Potassium nitrate (KNO_3) was purchased from Acros organics (New Jersey, USA). Potassium ferrocyanide trihydrate ($K_3Fe(CN)_6$) was purchased from EMD chemicals (Billerica, USA). Phosphate buffer saline (PBS) was purchased from Mediatech, Inc. (Manassas, USA). Alumina and diamond slurries were purchased from Bioanalytical Systems, Inc (BASi, Inc., West Lafayette, IN). Pt wire (99.95% Pt, 1.2 mm dia, 2 cm length) was obtained from Alfa Aesar (Ward Hill, MA). Silk cocoons were purchased from Mulberry Farms (Fallbrook, CA). Cellulose nanocrystals were acquired from the Process Development Center at The University of Maine (Orono, ME).

Equipment

Electrochemistry was performed on a BASi electrochemical cell stand with Pt/Ir working and counter electrodes and Ag/AgCl reference electrodes (BASi, West Lafayette, IN) or on an electrochemical impedance analyzer (ERZ100) and supporting software from eDAQ Inc (Colorado Springs, CO). All scanning white light interferometry (SWLI) was performed on a NewView 7300 3D optical surface profiler (Zygo Corporation (Middlefield, CT). Sonication for electrode cleaning was performed using a Model 150VT ultrasonic homogenizer (BioLogics Inc., Manassas, VA). Sonoelectrodeposition was performed using a DC power supply and an ultrasonic cleaner (Chicago Electric, Carol Stream, IL). Silk fibroin centrifugation was performed in a Beckman GPR centrifuge with GH-3.7 Horizontal Rotor (Beckman Coulter, Brea, California). PNIPAAM drying was performed in a vacuum oven (Squared Lab Line Instruments, Melrose Park, IL).

Graphene-Nanoplatinum Deposition

Platinum/iridium (80/20) electrodes (1.6 mm diameter) were decorated with graphene-platinum nanocomposite as described by Vanegas et al. (2014). Briefly, nanoplatinum was formed on the surface of each electrode via sonoelectrodeposition at 10 V for 90 seconds in a solution of 1.44 % (*w/v*) chloroplatinic acid and 0.002 % (*w/v*) lead acetate. A one ml aliquot of DI water was mixed with 2 mg of GO and 8 mg of L-ascorbic acid to form reduced graphene oxide (rGO). The suspension was ultrasonicated for 30 minutes. Immediately after sonication, a 2 µl aliquot of rGO was spin-coated on nPt-modified electrodes. The spin coat process included two cycles: the first cycle coats at 2621 rpm for 30 seconds, followed by coating at 5738 rpm for 60 seconds. After spin coating the rGO onto nPt, a second layer of nPt was electrodeposited on the surface of the modified electrode via sonoelectrodeposition at 10 V for 90 seconds. This nPt-rGO-nPt "sandwich" structure is denoted as PGP and specifically refers to spin-coat deposited rGO sandwiched between layers of platinum nanoclusters (nPt) as described in Vanegas et al. (2014). Vanegas et al (2014) provide details on the structural, electrochemical, and surface

View Article Online
DOI: 10.1039/C4AN01788A

chemistry for various architectures of graphene-nanoplatinum and CNT-nanoplatinum hybrid materials. Among these, "sandwich" structures for both hybrids yielded the highest electrochemical performance.

Hydrogel – Enzyme Nanocomposites

Chitosan hydrogels were prepared by dissolving chitosan (0.05 % *w/v*) in DI water, adding 0.008% (*w/v*) hydrochloric acid to solubilize the chitosan, and then vortex mixing at room temperature for 5 minutes. PNIPAAM hydrogels were synthesized by a radical polymerization reaction (Zhang et al. 2004). Briefly, NIPAAM monomer was dissolved in DI water to obtain a concentration of 6.7% (*w/w*) and then 2.0% (*w/w*) MBA (N,N-methylene-bisacrylamide) relative to NIPAAM was added. Free radical polymerization with 1.0 % (*w/w*) APS (Ammonium Persulfate) and TEMED (N,N,N',N'-Tetramethyl-ethylenediamine) was followed by immersion in DI water to leach reactants. Finally, the material was dried in a vacuum oven (Squared Lab Line Instruments, Melrose Park, IL) at room temperature at a pressure less than 13.3 kPa until all moisture was removed (approximately 24 hours). The resulting PNIPAAM solution had a concentration of 1.5 % (*w/v*). Silk hydrogel was created by extracting dead worms from silk cocoons, chopping the cocoons into small pieces (≈1 mm), and subjecting them to at least five one hour cycles of boiling and ultrasonication in DI water. The resulting suspension was then centrifuged at 1691g for 30 min. The supernatant liquid was further concentrated up to 1 % (*w/w*) solids and the hydrogel mixture was then vortex-agitated for 1 min at room temperature. CNC hydrogels (6.2% *w/w*) were directly used as purchased from the Process Development Center.

Enzyme-hydrogel composites were prepared by mixing 10 µl of AOx solution (14 U/mg suspended in PBS) with 10 µl of hydrogel, followed by vortex-agitation for 1 min at 25 °C. Hydrogel-enzyme-graphene-nanoplatinum composite electrodes were prepared by spin coating a 2 µl aliquot of the enzyme/hydrogel matrix onto PGP-modified electrodes by using the spin cycles previously described. The resulting biosensors are referred to as PGP_CHI (chitosan), PGP_PNI (PNIPAAM), PGP_CNC (CNC) and PGP_SILK (silk fibroin).

Electrochemical analysis and Imaging

To isolate the effects of hydrogel stimulus-response on electrochemical performance, all experiments were conducted at 25 °C and pH 7.10. Electrochemical characterization was performed using a three electrode cell stand according to Vanegas et al. (2014) and Chaturvedi et al. (2014). Cyclic voltammetry (CV) was carried out in 4 mM $Fe(CN)_6$/1 mM KNO_3 solutions at a switching potential of 600 mV versus a Ag/AgCl reference electrode with 5 seconds quiet time at scan rates of 50, 100, 150, and 200 mV/s. The electroactive surface area (ESA) was determined using the Randles-Sevcik equation (Eqn 1):

$$i_p=(2.69\times10^5)\, n^{3/2}\, D^{1/2}\, CAv^{1/2} \quad \text{(Eqn 1)}$$

where: i_p is the reduction peak (Amps) obtained from the cyclic voltammogram, n is the number of transferred electrons in the redox reaction, D is the diffusion coefficient ($cm^2\ sec^{-1}$), C is the molar

View Article Online
DOI: 10.1039/C4AN01788A

concentration of the working solution (mol cm^{-3}), A is the ESA of the electrode (cm^2) and *v* is the potential scan rate (V sec^{-1}). The constant term in Eqn 1 has the units of C mol $V^{0.5}$).

DC potential amperometry (DCPA) tests were conducted in 15 ml of PBS at a working potential of +500 mV versus a Ag/AgCl reference electrode with a sampling rate of 1 kHz. Electrodes were polarized for at least 1 hour, and current was measured at constant potential while successively injecting methanol in the stirred solution (450 rpm) at 2 minute intervals. The sensitivity, response time and lower limit of detection (LOD) were derived from DCPA time series plots using common methods in the literature (Vanegas et al., 2014; Chaturvedi et al., 2014).

Electrical impedance spectroscopy (EIS) was conducted in a solution of 4 mM $KFe(CN)_6$/1 mM KCl using a three electrode EA163 potentiostat and an eDAQ ERZ100. The applied potential was 100 mV (AC) and 0.25 mV (DC) with a frequency range of 1 Hz to 20 kHz. Analysis was performed on complex plane diagrams (Nyquist plots) generated by Z100. Equivalent circuit analysis was performed with Zman software.

SWLI was performed on a Zygo Newview 7100 optical surface profiler with a 20X by 2X objective using a gauss Spline filter (band-pass mode) with cut-off wavelength of 20 microns (low pass) and 0.83 microns (high pass).

Statistical Analysis

Analysis of variance (ANOVA model 1) and Tukey tests were performed using Minitab 17 software (Minitab Inc, State College, PA) to determine if electrode treatments produced significant differences ($p< 0.05$) in sensitivity, response time, or LOD. All experiments were based on a completely randomized design with at least three replications. All averages represent the arithmetic mean and all error bars represent the standard error of the mean based on Streiner et al (1996).

Results and Discussion

Electrochemical and imaging analysis were performed on each film and compared to bare Pt/Ir electrodes as well as PGP-modified electrodes. With the exception of silk, all of the hydrogels in this study are known to exhibit stimulus-response behavior; gel swelling is known to affect electron transport. To rule out structural changes as a contributing factor to electron transport during DCPA, the solution pH (7.07 ± 0.01) and temperature (25.0 ± 0.3 °C) were maintained constant throughout all experiments. Additionally, these operating conditions are expected for *in situ* autonomous monitoring under field conditions in the applications discussed herein.

Electrochemical analysis

Cyclic voltammetry was performed for six different electrodes including bare Pt/Ir, PGP, PGP_CHI, PGP_PNI, PGP_SILK, and PGP_CNC. Each of these treated electrodes demonstrated

View Article Online
DOI: 10.1039/C4AN01788A

reversible redox couples in potassium ferrocyanide. Representative CVs are shown in Figure 2a at a scan rate of 100 mV/sec and switching potential of 650 mV. Figure 2b shows the average ESA for each treated electrode ($n \geq 3$). As noted by Vanegas et al. (2014), PGP significantly improves electron transport relative to a bare Pt/Ir electrode; ESA values for PGP modified electrodes (0.21 ± 0.02 cm^2) were similar to Vanegas et al. (2014). This ESA is approximately fourteen times greater than a bare Pt/Ir electrode (0.015 ± 0.0004 cm^2). Although each of these four hydrogels has exhibited some conductivity in other studies, it was anticipated that addition of enzyme-hydrogel layers on PGP-modified electrodes would reduce the ESA due to the relatively high electron mobility in the PGP layer. For PGP_CNC, the reduction in ESA was significant, although the other hydrogels did not significantly reduce ESA. This was verified with analysis of variance (ANOVA) and a Tukey pairwise comparison. ANOVA revealed significant differences amongst the four PGP-hydrogel composites in terms of ESA ($p = 0.35$). Based on a Tukey pairwise comparison, chitosan (0.20 ± 0.06 cm^2), PNIPAAM (0.19 ± 0.02 cm^2) and silk (0.12 ± 0.02 cm^2) hydrogels were not significantly different compared to a PGP electrode at the 95% confidence interval. Conversely, PGP_CNC (0.09 ± 0.03 cm^2) was significantly lower than PGP at the 95% confidence interval, but higher than a bare Pt/Ir electrode.

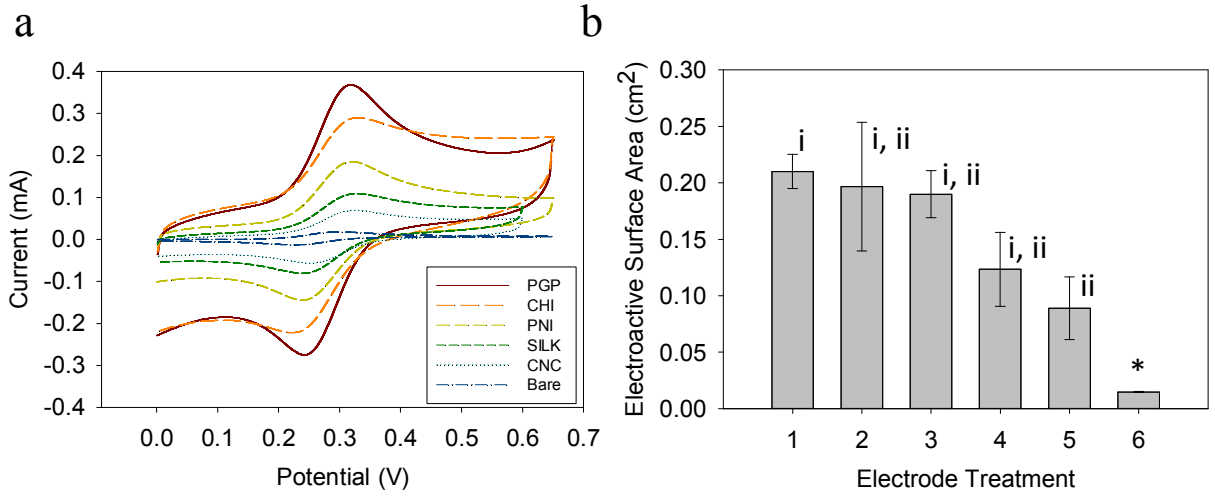

Figure 2. Electroactive surface area of various hydrogel-graphene-AOx bionanocomposites. a) Representative cyclic voltammograms at a scan rate of 100 mV/sec and switching potential of 650 mV. b) Average electroactive surface area for all electrodes compared to a bare Pt/Ir electrode and an electrode modified with PGP nanocomposite ($n > 3$). 1=PGP, 2=PGP_CHI, 3=PGP_PNI, 4=PGP_SILK, 5=PGP_CNC, 6=Bare Pt/Ir. Groups i and ii exhibit statistical differences ($p < 0.05$) based on a Tukey pairwise comparison. *Bare Pt/Ir electrode is shown for comparison.

Figure 3a shows a representative Nyquist plot for bare Pt/Ir, PGP, and PGP_CHI electrodes at a potential of 100 mV (AC), 0.25 mV (DC) and frequency range of 1 Hz-100 kHz. Bare Pt/Ir electrodes exhibit slow electron transfer, indicated by the semicircular region in the faradaic impedance spectrum (Kaushik et al., 2010; Wang et al., 2014). The charge transfer resistance for bare Pt/Ir (9.3 ± 1.9 kΩ) is significantly higher than the modified electrodes. Conversely, no semicircular region was measureable for PGP and PGP-hydrogel bionanocomposite electrodes (inset in Figure 3a and Figure 3b), indicating fast

View Article Online
DOI: 10.1039/C4AN01788A

electron transfer with negligible charge transfer resistance. Zman™ software (eDAQ Inc.) was used to estimate the charge transfer resistance (R_{ct}) based on the Randles-Ershler equivalent circuit model (Figure 3c). The Chi squared values for all electrodes (1.3×10^{-3} to 3.9×10^{-3}) were similar (see supplemental Table S1) indicating a good fit to the equivalent circuitry. Charge transfer resistance in chitosan, PNIPAAM, CNC and silk nanocomposites were not statistically different than PGP electrodes based on ANOVA ($p = 0.23$). The solution resistance (R_s) did not significantly change for any of the electrodes tested except the bare electrodes (see supplemental Table S1). The trends in Figure 3d are similar to ESA data for each electrode (Figure 2b); validating excellent charge transfer resistance in all PGP modified electrodes relative to a bare Pt/Ir electrode. This supports the finding by Vanegas et al. (2014), and extends the concept to include PGP-hydrogel-enzyme bionanocomposites.

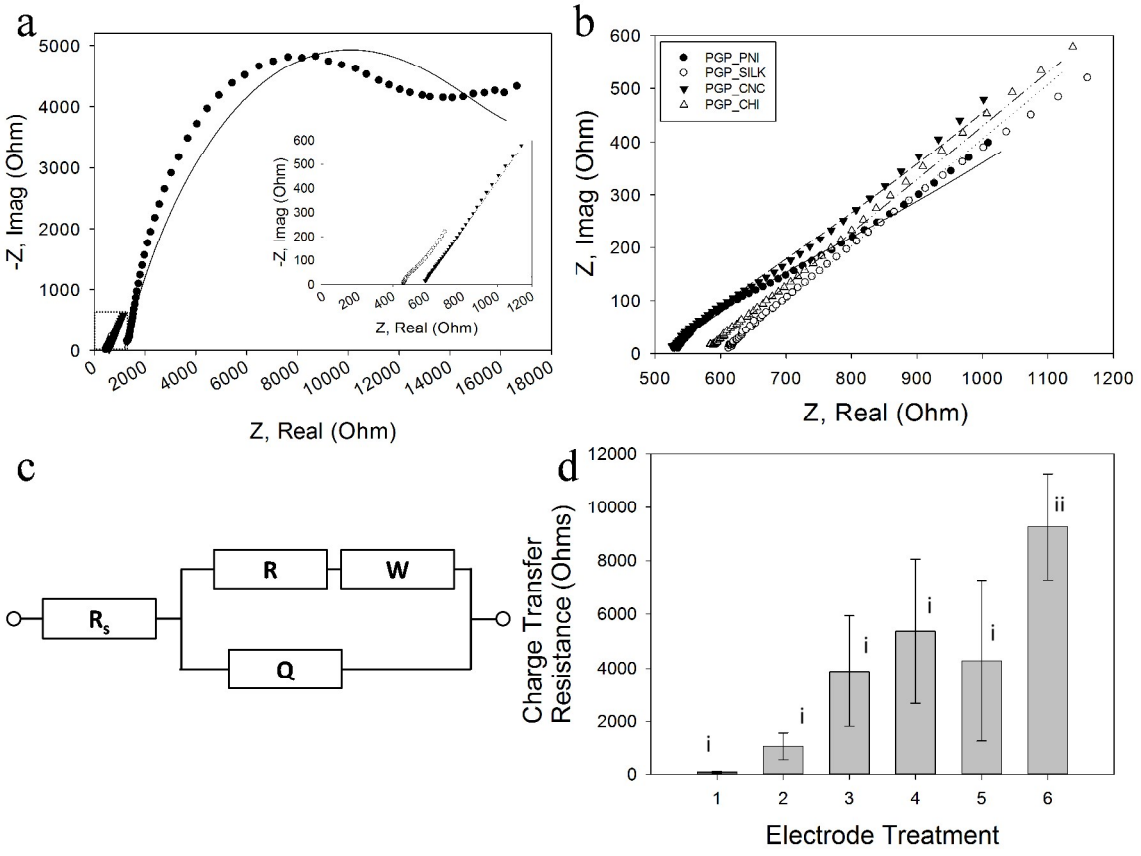

Figure 3. Electron transfer kinetics determined with EIS for various hydrogel-graphene-AOx bionanocomposites. a) Representative Nyquist plots for bare Pt/Ir (black circles), PGP (white circles) and PGP_CHI (black triangles). Solid lines indicate fitting data to equivalent circuit. Inset shows exploded view of PGP and PGP_CHI electrodes. b) Nyquist plots for PGP_CHI, PGP_PNI, PGP_SILK and PGP_CNC treated electrodes. c) Randles-Ershler equivalent circuit used to derive solution resistance (Rs) and charge transfer resistance (R). d) Average charge transfer resistance for treated electrodes; 1=PGP, 2=PGP_CHI, 3=PGP_PNI, 4=PGP_SILK, 5=PGP_CNC, 6=Bare.

View Article Online
DOI: 10.1039/C4AN01788A

Figures 2 and 3 indicate that chitosan and PNIPAAM had a higher permeability to charged ions than fibroin and CNC hydrogels, which indicates that both have a more porous structure network relative to fibroin and CNC hydrogels under the same experimental conditions. This is based on the assumption that permeable structure, or lightly crosslinked networks, have higher permeability relative to dense, highly crosslinked network as shown by others using first order kinetic models (Murphy et al., 1992; Sung et al., 2014; Zhao et al., 2012).

Imaging

Figure 4a shows a representative SWLI image of a PGP_CHI treated surface. Chitosan and PNIPAAM treatments formed films with feature sizes on the order of 550 to 750 nm, while Silk and CNC treatments formed relatively smooth surfaces with feature sizes (50 to 200 nm) an order of magnitude lower (see supplemental Figure S1 for all SWLI images). The average root mean square roughness (RMS) data for all electrodes (Figure 4b) shows that chitosan (699.5 ± 113.2 µm) and PNIPAAM (712.6 ± 31.4 µm) treatments were not statistically different than PGP alone (587.0 ± 63.4 µm) (group a). However, the surface roughness of PGP_CNC treated electrodes (44.8 ± 0.8 µm) was significantly lower than PGP based on Tukey pairwise comparison. Electrodes treated with PGP_SILK (267.9 ± 144.2 µm) were not statistically different than groups i and ii. These trends are similar to the ESA and EIS data (Figures 2-3), with the exception of PGP_SILK. The low RMS for silk nanocomposites may be due the formation of micellular microstructures as noted by Hu et al. (2010) and Jin et al. (2003). Increased surface roughness is associated with improved ESA and decreased charge transfer resistance due to the increase in radial electron transport. The mechanism for increased charge transfer due to nanoscale roughness features is a radial transport term ($i_{radial} = nFACD^{*}r^{-1}$) which contributes in a summative fashion to planar transport (i_{planar} =nFACD$^{0.5}$ * πt^{-1}) where: i_{radial} is the reduction peak (amps) obtained from the cyclic voltammogram, n is the number of transferred electrons in the redox reaction, F is the Faraday constant (C mol V$^{0.5}$), A is the electroactive surface area of the electrode (cm^2), C is the molar concentration of the working solution (mol cm^{-3}), D is the diffusion coefficient (cm^2 sec^{-1}), r is the radius of the radial diffusion layer (cm), and t is the depth of the planar diffusion layer (cm) (Gmucová et al., 2012).

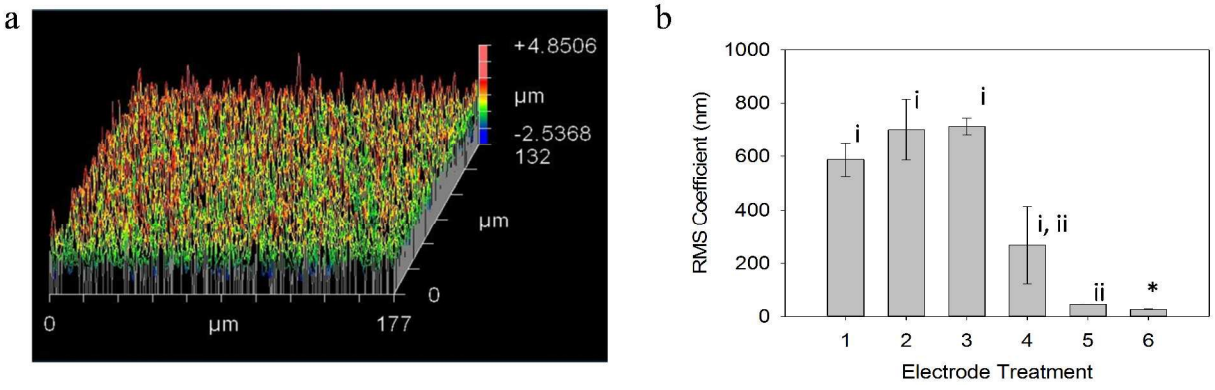

Figure 4. a) Representative SWLI oblique map of PGP_CHI electrode. b) Average root mean square surface roughness coefficient for all bionanocomposites (n > 3). 1=PGP (RMS = 587.0 ± 63.4 nm),

View Article Online
DOI: 10.1039/C4AN01788A

2=PGP_CHI (RMS = 699.5 ± 113.2 nm), 3=PGP_PNI (RMS = 712.6 ± 31.4 nm), 4=PGP_SILK (RMS = 267.9 ± 144.2 nm), 5=PGP_CNC (RMS = 44.8 ± 0.8 nm), 6=Bare (RMS = 25.89 ± 1.83 nm). Electrodes with chitosan, PNIPAAM, and silk fibroin hydrogels have significantly higher surface roughness (group a) than those treated with CNC (group b), while PGP electrodes coated with silk hydrogel show a slight decrease in surface roughness that is not statistically different than groups i and ii. *Bare Pt/Ir electrode is shown for comparison.

The variations in electron transport and morphology observed in Figures 2-4 can be linked to pH and temperature during experimentation. Solution pH plays an important role in conductivity of polyelectrolytic hydrogels by formation of acidic groups on the surface. For chitosan, PNIPAAM and CNC, temperature induces structural changes which regulate gel porosity. Under the experimental conditions (pH = 7.1 and 25 °C), chitosan (pI = 6.5) and PNIPAAM (pI = 6.2) hydrogels are macroporous, but are expected to be deprotonated (López-León et al., 2005; de Alvarenga, 2011; Zhang and Peppas, 2000; Anirudhan et al., 2013). At pH 7.1, fibroin hydrogels (pI ≈ 3.7) are deprotonated negatively charged and macroporous after transition from amorphous to the β-sheet allotrope (Foo et al., 2006; Zhang et al., 2000). The heterogenous charge density of hydrogel/AOx composites on PGP nanostructures is not known, and further studies are needed to explore these fundamental material properties. However, the electrochemical data in Figures 2 and 3 suggest that the polymer network is positively charged. Under these experimental conditions CNC (pI = 6.5), is deprotonated, but film dispersion may lead to relatively poor performance, as CNC is known to have excellent dispersion in water (Liang et al., 2007). Based on the work by Dufresne (2010), it was anticipated that AOx would serve as a reinforcing structure for CNC via CBM and carboxyl-amine binding, leading to formation of a stable hydrogel. However, additional studies are needed to understand the mechanical properties and stability of CNC-oxidase composite films.

Biosensor efficacy

AOx oxidizes short chain alcohols, producing carbonyl compounds and hydrogen peroxide; free electrons produced during the deprotonation of hydrogen peroxide are measured as oxidative current at +500mV (see supplemental Figure S2). To investigate the efficacy of each hydrogel-graphene bionanocomposite, AOx biosensors were tested in PBS at 25°C and pH 7.07 ± 0.01 using DCPA. A representative DCPA time series is shown in Figure 5a for PGP_CHI, and the inset shows the calibration plot (see supplemental Figure S3 for an exploded view of inset). After stepwise addition of methanol, oxidative current increased until a steady state response was established. Figure 5b shows the average sensitivity values derived from calibration curves for all four bionanocomposites. Performance characteristics extracted from this curve include sensitivity (Figure 5b), response time (Figure 5c), and limit of detection (Figure 5d).

Among the various hydrogel nanocomposites, the highest sensitivity toward methanol was observed for electrodes prepared with chitosan (0.46 ± 0.18 μA mM^{-1} and PNIPAAM (0.30 ± 0.11 μA mM^{-1}). These treatments also yielded the fastest response times (4.33 ± 0.82 s for CHI and 4.77 ± 1.1 s for PNIPAAM). In contrast, PGP_SILK and PGP_CNC showed the lowest sensitivity (0.09 ± 0.02 μA mM^{-1}

View Article Online
DOI: 10.1039/C4AN01788A

for SILK, and 0.15 ± 0.03 μA mM^{-1} for CNC) and slowest response times (8.9 ± 2.1 for SILK, and 6.3 ± 0.8 s for CNC). Detection limits for chitosan (0.1 ± 0.02 μM), PNIPAAM (0.09 ± 0.3 μM), silk (0.09 ± 0.03 μM), and CNC (0.07 ± 0.01 μM) were all within ranges that were relevant for industrial applications such as forensics, food and beverage, and biofuel industries. Sensitivity, response time and limit of detection for all four electrode treatments were not statistically different based on ANOVA analysis (p = 0.64 for sensitivity, p = 0.50 for response time, and p = 0.77 for limit of detection).

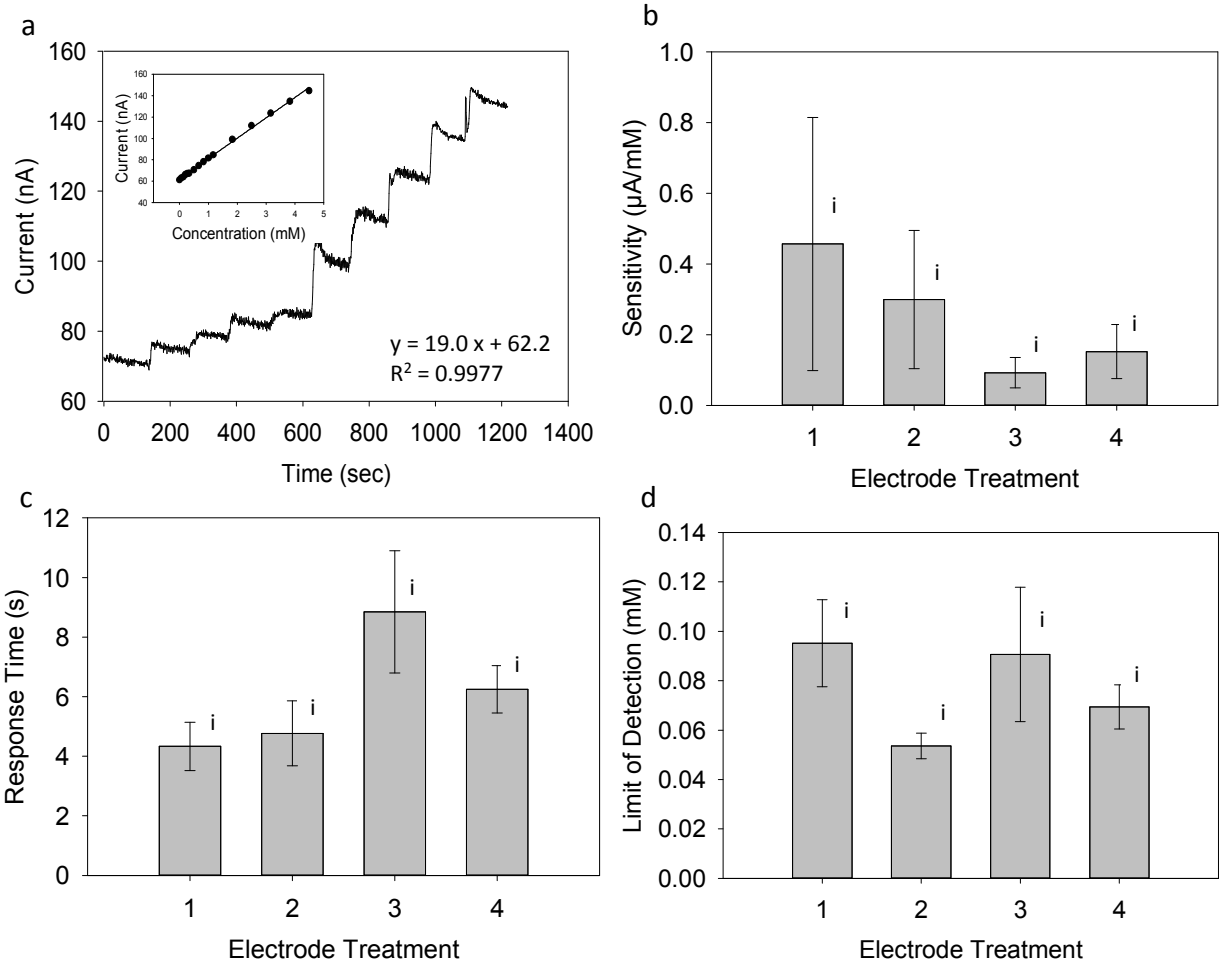

Figure 5. DC potential amperometry for treated electrodes. (a) A representative DCPA time series for AOx immobilized in chitosan on a PGP-modified electrode (inset shows average current versus methanol concentration; see supplemental information for expanded plot) (b) Average sensitivity, (c) average response time and (d) average limit of detection for each electrode treatment (n ≥ 3). 1=PGP_CHI, 2=PGP_PNI, 3=PGP_SILK, 4=PGP_CNC. A Tukey pairwise comparison was used to group electrodes with no statistically significant differences in performance (indicated by the letter a).

Hysteresis (measured as percent difference in polarization current after exposure to methanol) varied from 18 ± 7% for CNC treated electrodes to 54 ± 8% for silk treated electrodes. Hysteresis for chitosan (32 ± 8%) and PNIPAAM (49 ± 20%) nanocomposites was less than that of silk, but higher than

View Article Online
DOI: 10.1039/C4AN01788A

CNC (average hysteresis for all electrodes was 38 ± 8%). Hysteresis for the four electrode treatments was not statistically different based on ANOVA analysis and Tukey Tests (p=0.22 for hysteresis) (see supplemental figure S4). Shelf life of all bionanocomposites varied considerably; between 65% and 92% reduction in sensitivity after 100 days of storage in PBS at 4º C. The sensitivity of CHI electrodes decreased by 41.2% after 90 days, while sensitivity of PNI and CNC electrodes reduced by 84.2%, and 85.5%, respectively (see Figure S5). The sensitivity of SILK treated electrodes after 100 days at 4º C was similar to as prepared electrodes. These data indicate that CHI and SILK may be the best materials for development of robust AOx bionanosensors; CHI is the clear candidate between these two materials for superior performance. If shelf life is not a design consideration, CHI or PNI bionanohybrid electrodes are both strong candidates using the configurations described herein. These two hydrogels have distinct stimulus-response properties that can be exploited in future studies: CHI is a pH-responsive polymer while PNI is a temperature-responsive polymer.

Comparison to other AOx hydrogel biosensors

The performance characteristics of the hydrogels investigated here are within the range of other devices in the published literature, and some properties are significantly improved (Table 1). Of particular importance is that the single enzyme bionanocomposites developed in this study are biocompatible/non-toxic, and did not use mediators or cofactors. These are very important attributes for application in food and beverage industry (where release of noxious or toxic compounds is strictly prohibited) and also in biofuel reactor monitoring (where addition of mediators is not cost effective at the scale of analysis). The hydrogel-graphene bionanocomposites also demonstrated excellent response times; the biosensors in this study were at least an order of magnitude faster than previously published sensors.

Table 1. Comparison of hydrogel immobilization approaches for alcohol oxidase biosensors.

Hydrogel	**Sensitivity [μA mM^{-1}]**	**LOD [μM]**	**Response Time [s]**	**Linear range [μM]**	**Reference**
AOx/HRP/ polyvinyl imidazole osmium	1.31 ± 0.06	10 ± NR	NR	250 to 2000	Vijayakumar et al. (1996)
PCS *(a)*	0.03 ± 0.0002	26 ± NR	12 ± 0.7	100 to 3000	Patel et al. (2001)
HRP/PVI-Os/PEG-DGE *(a)*	0.10 ± NR	20 ± NR	NR	NR	Alpeeva et al. (2005)
AOx/chitosan/ Eggshell *(a)*	*(b)*	30 ± NR	1.0 ± NR	60 to 800	Wen et al. (2007)
PAMAM *(a)*	0.34 ± NR	16 ± NR	100 ± NR	25 to 1000	Akin et al. (2010)

View Article Online
DOI: 10.1039/C4AN01788A

PEI *(a)*	0.91 ± NR	5 ± NR	55 ± NR	8 to 42	Das et al. (2013)
Chitosan_PGP	0.46 ± 0.18	100 ± 20	4.33 ± 0.8	100 to 2500	this work
PNIPAAM_PGP	0.30 ± 0.11	50 ± 10	4.77 ± 1.1	50 to 2500	this work
Silk_PGP	0.09 ± 0.02	90 ± 300	8.85 ± 2.1	90 to 2500	this work
CNC_PGP	0.15 ± 0.03	70 ± 10	6.30 ± 0.8	70 to 2500	this work

(a): sensor tested with ethanol, but shown for comparison.

(b): sensitivity (3.02 ± NR mg-O_2 L^{-1} mM-EtOH) was shown as decrease in dissolved oxygen.

NR indicates data not reported

Patel et al. (2001) and Vijayakumar et al. (1996) developed some of the first successful AOx biosensors. The single enzyme system immobilized AOx in poly(carbamoyl)sulfonate (PCS) hydrogel (Patel et. al., 2001). The sensor had a relatively low sensitivity (0.03 μA mM^{-1}), although the LOD (26 μM), response time (12 sec), and range (100 to 3000 μM) were comparable to most devices published to date. The bi-enzyme sensor develop by Vijayakumar et al. (1996) showed excellent sensitivity (1.31 μA mM^{-1}), LOD (10 μM), and range (10 to 4000 μM), and in many ways is one of the best sensors to date. However, the use of osmium complexes as a mediator has some problems for applications in biological samples such as food and biofuel production. Lukasova et al. (1982) and others have shown that osmium complexes with ssDNA and dsDNA, which may lead to poor selectivity in samples where polynucleotides are present. Furthermore, the tetroxide form of osmium is highly toxic (Wheeldon et al., 2008), which could lead to contamination of samples (or processors in the case of biofuel reactors). Another drawback of the device by Vijayakumar et al. (1996) is the need for two enzymes, which is suspected to lead to poor shelf life (although no data is reported beyond 7 days).

Wen et al. (2007) developed an AOx device using a chitosan/eggshell membrane composite as the encapsulant. The LOD (30 μM) and response time (1 sec) were excellent. The sensitivity toward ethanol cannot be compared to other devices because the sensor output was recorded as a decrease in dissolved oxygen concentration (rather than directly using DCPA as other studies have done). The detection of oxygen consumption as a surrogate for direct measurement of ethanol is challenging for the applications discussed here because samples taken from food/beverage products or biogas reactors have variable background oxygen concentration. Furthermore, any contamination of the sensor surface with a living microorganism which undergoes aerobic metabolism imparts significant bias in the measured signal (on the order of 100-1000 times higher than the oxidase activity of the enzyme based on approximations of oxidoreductase distribution in cells).

View Article Online
DOI: 10.1039/C4AN01788A

A bi-layer, bi-enzyme sensor developed by Alpeeva et al. (2005) combined horseradish peroxidase (HRP) or royal palm tree peroxidase combined with AOx from a genetically modified strain of the methylotrophic yeast *Hansenula polymorpha* in hydrogel layers encapsulated in polyvinyl imidazole (PVI). The bi-enzyme sensor had a sensitivity that was relatively low (0.10 μA mM^{-1}), but a relatively low LOD (20 μM) and high stability (measured based on a Michaelis deactivation constant). Response time and linear range were not reported for this device.

A multiplexing device developed by Akin et al. (2010) was constructed with an AOx/glutaraldehyde/cysteamine/PAMAM composite on a gold electrode by self-assembly. Although this device was used to measure ethanol, oxygen, and glucose, the ethanol biosensor used AOx, and is therefore used for comparison. The sensitivity (0.34 μA mM^{-1}) and low LOD (16 μM) for the PAMAM device were attributed to efficient crosslinking between cysteamine and the poly(amido amine) (PAMAM) dendrimers (Akin et al., 2010). The device also showed a wide sensing range (25 to 1000 μM) and a relatively low LOD (100 μM). The challenge with using the design by Akin et al. (2010) in food and beverage or biofuel applications is the cytotoxicity of PAMAM dendrimers (Akin et. al., 2010). It is also not possible to directly assess the reliability of this device for applications due to the lack of replication in many of the reported data.

A design was recently published by Das et al. (2013), which involved deposition of AOx in polyethyleneimine (PEI) onto a gold electrode coated with multiwalled carbon nanotubes (MWCNT) suspended in Nafion at pH 7.5. This design demonstrated a good sensitivity (0.91 μA mM^{-1}) and LOD (5 μM) for argon purged solutions, although replicates were not reported for some of the data sets and no statistical validation could be conducted. The extremely low LOD was attributed to high enzymatic activity due to efficient amine bonding of AOx along positively charged PEI chains. Drawbacks of this design are the relatively poor linear range (8 to 42 μM), cytotoxicity of PEI chains, and that the working solution must be purged with argon prior to analysis (which is challenging in field studies). The cytotoxicity is a major concern for analysis of alcohols in food products since PEI is soluble in methanol (Liu et al., 2012). Although no leaching studies were conducted for the PEI device (Das et. al., 2013), dispersion of long chain PEI fractions during measurement could contaminate food products and/or biofuel reactors.

The hydrogels used in this study are water soluble, biocompatible, and non-toxic. Although detailed selectivity tests were not conducted in this study, AOx from *Pichia pasotoris* has a high affinity for methanol, and is also known to oxidize propargyl alcohol (90% selective relative to methanol), ethanol (82% selective), and 2-propanol (81% selective) (Sahm et al., 1982). Future studies focusing on tuning of the hydrogel to meet specific application requirements (e.g., stimuli-response properties, durability, etc.) may significantly improve performance, although characterization of the rheological and stimuli-response properties is outside of the scope of this work.

Vijayakumar et al. (1996) showed that bi-enzyme electrodes using polyvinyl imidazole osmium as the encapsulant can be stored for up to 7 days, and sensors are stable for up to 8 hours of continuous measurement. The stability and shelf life of all hydrogels was significantly better than the 8 days reported by Vijayakumar et al. (1996). Comparison to other sensors in the literature is difficult as hysteresis and shelf life are not commonly reported.

View Article Online
DOI: 10.1039/C4AN01788A

Conclusions

Electroactive surface area, impedance spectra, amperometric sensitivity, response time, limit of detection and gel morphology were measured to quantitatively compare alcohol biosensors composed of enzyme-hydrogel-graphene bionanocomposites. The sensitivity, limit of detection, and range for all hydrogels composites in this study were within the range of other devices in the published literature. Response time and shelf life were significantly improved over other published devices. Based on the six performance parameters tested, biosensors composed of PNIPAAM and chitosan were the most efficient at pH 7.1 and 25°C. The highest shelf life was observed for biosensors prepared with chitosan and silk, although overall nanohybrid AOx sensors based on silk hydroges were relatively poor. AOx biosensors based on CNC hydrogels had the lowest performance of the four materials tested. Overall, electrodes prepared with chitosan and PNIPAAM hydrogels were the most efficient. These two hydrogels have distinct stimulus-response properties that can be exploited in future studies based on actuation of the nanohybrid material for sensing applications. Of particular importance is that the single enzyme bionanocomposites developed in this study are all biocompatible/non-toxic, and did not use mediators or cofactors. These are very important attributes for application in the food and/or biofuel industries. Evaluation of these materials in a side-by-side comparison provides insight into the mechanisms of enzyme-hydrogel nanomaterial interactions and the effect(s) on general biosensor performance for other oxidase with a similar pKa.

Acknowledgements

The authors gratefully acknowledge the Florida Space Grant Consortium Seed Fund (#00091356), the UF ABE Graduate Assistantship (Burrs), the UF/FAMU Feeder Fellowship (Burrs), the Colciencias Fellowship (Vanegas), and the UF Early Career Award for financial support.

View Article Online
DOI: 10.1039/C4AN01788A

References

1. E. M. Ahmed, J. Adv. Res., 2013.

2. M. Akin, A. Prediger, M. Yuksel, T. Höpfner, D. O. Demirkol, S. Beutel, S. Timur, and T. Scheper, Biosens. Bioelectron., 2011, 26, 4532–7.

3. E. Akyilmaz and E. Dinçkaya, Biosens. Bioelectron., 2005, 20, 1263–9.

4. I. S. Alpeeva, A. Vilkanauskyte, B. Ngounou, E. Csöregi, I. Y. Sakharov, M. Gonchar, and W. Schuhmann, Microchim. Acta, 2005, 152, 21–27.

5. T. S. Anirudhan and S. R. Rejeena, Carbohydr. Polym., 2013, 93, 518–27.

6. M. Badea, A. Curulli, and G. Palleschi, Biosens. Bioelectron., 2003, 18, 689–698.

7. H. Bai, K. Sheng, P. Zhang, C. Li, and G. Shi, J. Mater. Chem., 2011, 21, 18653.

8. M. Boujtita, J. P. Hart, and R. Pittson, Biosens. Bioelectron., 2000, 15, 257–63.

9. D. Buenger, F. Topuz, and J. Groll, Prog. Polym. Sci., 2012, 37, 1678–1719.

10. J. Cai, S. Kimura, M. Wada, and S. Kuga, Biomacromolecules, 2009, 10, 87–94.

11. D. Carelli, D. Centonze, A. De Giglio, M. Quinto, and P. G. Zambonin, Anal. Chim. Acta, 2006, 565, 27–35.

12. P. Chaturvedi, D. C. Vanegas, M. Taguchi, S. L. Burrs, P. Sharma, and E. S. McLamore, Biosens. Bioelectron., 2014, 58, 179–85.

13. C.-S. Cho, ISRN Mater. Sci., 2012, 2012, 1–24.

14. J. C. Claussen, A. Kumar, D. B. Jaroch, M. H. Khawaja, A. B. Hibbard, D. M. Porterfield, and T. S. Fisher, Adv. Funct. Mater., 2012, 22, 3399–3405.

15. M. Das and P. Goswami, Bioelectrochemistry, 2013, 89, 19–25.

16. A. G.-V. de Prada, N. Peña, M. L. Mena, a. J. Reviejo, and J. M. Pingarrón, Biosens. Bioelectron., 2003, 18, 1279–1288.

17. A. Dufresne, Molecules, 2010, 15, 4111–28.

18. J. V. Edwards, N. Prevost, A. French, M. Concha, A. Delucca, and Q. Wu, Eng. Sci. Res., 2013, 2013, 20–28.

19. C. W. P. Foo, E. Bini, J. Hensman, D. P. Knight, R. V. Lewis, and D. L. Kaplan, Appl. Phys. A, 2005, 82, 223–233.

20. E. S. Gil, D. J. Frankowski, R. J. Spontak, and S. M. Hudson, Biomacromolecules, 2005, 6, 3079–87.

View Article Online
DOI: 10.1039/C4AN01788A

21. K. Gmucová, in Electrochemical Cells- New Advances in Fundamental Researches and Applications, 2012, pp. 3–16.

22. F. M. Goycoolea, M. E. Fernández-Valle, I. Aranaz, and Á. Heras, Macromol. Chem. Phys., 2011, 212, 887–895.

23. H. Gülce, a Gülce, M. Kavanoz, H. Coşkun, and a Yildiz, Biosens. Bioelectron., 2002, 17, 517–21.

24. L. He, D. Lin, Y. Wang, Y. Xiao, and J. Che, Colloids Surf. B. Biointerfaces, 2011, 87, 273–9.

25. S. Hrapovic, Y. Liu, K. B. Male, and J. H. T. Luong, Anal. Chem., 2004, 76, 1083–1088.

26. X. Hu, Q. Lu, L. Sun, P. Cebe, X. Wang, X. Zhang, and D. L. Kaplan, Biomacromolecules, 2010, 11, 3178–88.

27. E. Jang and W.-G. Koh, Sensors Actuators B Chem., 2010, 143, 681–688.

28. E. Jang, K. J. Son, B. Kim, and W.-G. Koh, Analyst, 2010, 135, 2871–8.

29. H.-J. Jin and D. L. Kaplan, Nature, 2003, 424, 1057–61.

30. A. Kaushik, P. R. Solanki, K. Kaneto, C. G. Kim, S. Ahmad, and B. D. Malhotra, Electroanalysis, 2010, 22, 1045–1055.

31. J. Kim and S. Yun, Macromolecules, 2006, 39, 4202–4206.

32. J.-H. Kim, S. Mun, H.-U. Ko, G.-Y. Yun, and J. Kim, Nanotechnology, 2014, 25, 092001.

33. S. Kiralp, A. Topcu, G. Bayramoğlu, M. Y. Arıca, and L. Toppare, Sensors Actuators B Chem., 2008, 128, 521–528.

34. C. N. Kotanen, C. Tlili, and A. Guiseppi-Elie, Talanta, 2013, 103, 228–35.

35. B. Krajewska, Enzyme Microb. Technol., 2004, 35, 126–139.

36. K. H. Lee, C. S. Ki, D. H. Baek, G. D. Kang, D. Ihm, and Y. H. Park, Fibers Polym., 2005, 6, 181–185.

37. A. Levasseur, E. Drula, V. Lombard, P. M. Coutinho, and B. Henrissat, Biotechnol. Biofuels, 2013, 6, 41.

38. H. Liu, J. Qian, Y. Liu, T. Yu, and J. Deng, Bioelectrochemistry Bioenerg., 1996, 39, 303–308.

39. K. Liu, X. Wang, W. Fan, Q. Zhu, J. Yang, J. Gao, and S. Gao, Int. J. Nanomedicine, 2012, 7, 1149–62.

40. T. López-León, E. L. S. Carvalho, B. Seijo, J. L. Ortega-Vinuesa, and D. Bastos-González, J. Colloid Interface Sci., 2005, 283, 344–51.

41. E. Lukasavo, F. Jelen, and E. Palecek, Gen. Physiol. Biophys., 1982, 1, 53–70.

View Article Online
DOI: 10.1039/C4AN01788A

42. N. D. Luong, N. Pahimanolis, U. Hippi, J. T. Korhonen, J. Ruokolainen, L.-S. Johansson, J.-D. Nam, and J. Seppälä, J. Mater. Chem., 2011, 21, 13991.

43. Y. Miao and S. N. Tan, Analyst, 2000, 125, 1591–1594.

44. S. M. Murphy, C. J. Hamilton, M. L. Davies, and B. J. Tighe, Biomaterials, 1992, 13, 979–990.

45. M. Niculescu, R. Mieliauskiene, V. Laurinavicius, and E. Csöregi, Food Chem., 2003, 82, 481–489.

46. R. Pauliukaite, M. E. Ghica, O. Fatibello-Filho, and C. M. a. Brett, Electrochim. Acta, 2010, 55, 6239–6247.

47. R. Pelton, TrAC Trends Anal. Chem., 2009, 28, 925–942.

48. R. S. Reiner and A. W. Rudie, in Production and Application of Cellulose Nanomaterials, eds. M. Postek, R. Moon, A. Rudie, and M. Bilodeau, 1998.

49. M.-R. Sahm, Hermann; Schutte, Horst; Kula, Methods Enzymol., 1982, 89, 424–428.

50. Y. Shao, J. Wang, H. Wu, J. Liu, I. A. Aksay, and Y. Lin, Electroanalysis, 2010, 22, 1027–1036.

51. D. L. Streiner, Can. J. Psychiatry, 1996, 498–502.

52. W. Suginta, P. Khunkaewla, and A. Schulte, Chem. Rev., 2013, 113, 5458–79.

53. C. Sung, K. Hearn, and J. Lutkenhaus, Soft Matter, 2014, 10, 6467–6476.

54. H. Tao, D. L. Kaplan, and F. G. Omenetto, Adv. Mater., 2012, 24, 2824–37.

55. D. C. Vanegas, M. Taguchi, P. Chaturvedi, S. Burrs, M. Tan, H. Yamaguchi, and E. S. McLamore, Analyst, 2014, 139, 660–7.

56. D. Wang, F. Li, J. Zhao, W. Ren, Z. Chen, J. Tan, Z. Wu, I. Gentle, G. Q. Lu, and H. Cheng, ACS Nano, 2009, 3, 1745–1752.

57. W. Wang, S. Guo, I. Lee, K. Ahmed, J. Zhong, Z. Favors, F. Zaera, M. Ozkan, and C. S. Ozkan, Sci. Rep., 2014, 4, 4452.

58. W. Wang, W. Xiong, J. Wan, X. Sun, H. Xu, and X. Yang, Nanotechnology, 2009, 20, 105103.

59. G. Wen, Y. Zhang, S. Shuang, C. Dong, and M. M. F. Choi, Biosens. Bioelectron., 2007, 23, 121–9.

60. Z. Weng, Y. Su, D.-W. Wang, F. Li, J. Du, and H.-M. Cheng, Adv. Energy Mater., 2011, 1, 917–922.

61. I. R. Wheeldon, J. W. Gallaway, S. C. Barton, and S. Banta, Proc. Natl. Acad. Sci. U. S. A., 2008, 105, 15275–80.

62. X. J. Wu, M. M. F. Choi, C. S. Chen, and X. M. Wu, Biosens. Bioelectron., 2007, 22, 1337–44.

63. Y. Wu, Z. Dou, Y. Liu, G. Lv, T. Pu, and X. He, RSC Adv., 2013, 3, 12726.

View Article Online
DOI: 10.1039/C4AN01788A

64. M.-Y. Yen, C.-C. Teng, M.-C. Hsiao, P.-I. Liu, W.-P. Chuang, C.-C. M. Ma, C.-K. Hsieh, M.-C. Tsai, and C.-H. Tsai, J. Mater. Chem., 2011, 21, 12880.

65. W. W. Yu and I. M. White, Anal. Chem., 2010, 82, 9626–30.

66. M. Yuan, A. Liu, M. Zhao, W. Dong, T. Zhao, J. Wang, and W. Tang, Sensors Actuators B Chem., 2014, 190, 707–714.

67. L. Zhai, Chem. Soc. Rev., 2013, 42, 7148–60.

68. J. Zhang and N. A. Peppas, Macromolecules, 2000, 33, 102–107.

69. X.-Z. Zhang, D.-Q. Wu, and C.-C. Chu, Biomaterials, 2004, 25, 3793–805.

70. Z. Zhang, T. Jiang, K. Ma, X. Cai, Y. Zhou, and Y. Wang, J. Mater. Chem., 2011, 21, 7705.

71. X. Zhao, Y. Liu, J. Lu, J. Zhou, and J. Li, Chemistry, 2012, 18, 3687–94.

View Article Online
DOI: 10.1039/C4AN01788A

Supplemental information

Table S1. Equivalent circuit analysis of Nyquist plots for various electrode configurations. EIS data was analyzed with the Randles-Ershler model. Results are shown for charge transfer resistance (R), solution resistance (R_s), Capacitance (Q_v and Q_a), Warburg impedance (W) and Chi-squared (ChiSq).

Table S1. Nyquist Simulation Results

	Bare Platinum	PGP	PGP + CHI + AOX	PGP + PNI + AOX	PGP + SILK + AOX	PGP + CNC + AOX
R (Ω)	9.27E+03	7.24E+03	1.08E+03	3.88E+03	5.37E+03	4.28E+03
R_s (Ω)	1.53E+03	7.79E+02	4.60E+02	6.07E+02	6.30E+02	7.22E+02
Q_v	6.85E-05	6.37E-04	3.61E-04	7.37E+02	2.38E-04	1.15E+01
Q_a	3.42E-06	1.50E-04	4.30E-04	2.58E-04	3.20E-04	2.40E-04
W	7.59E-01	6.92E-01	5.89E-01	5.82E-01	6.12E-01	6.20E-01
ChiSq	3.38E-03	3.45E-03	3.24E-03	3.92E-03	2.79E-03	1.30E-03

View Article Online
DOI: 10.1039/C4AN01788A

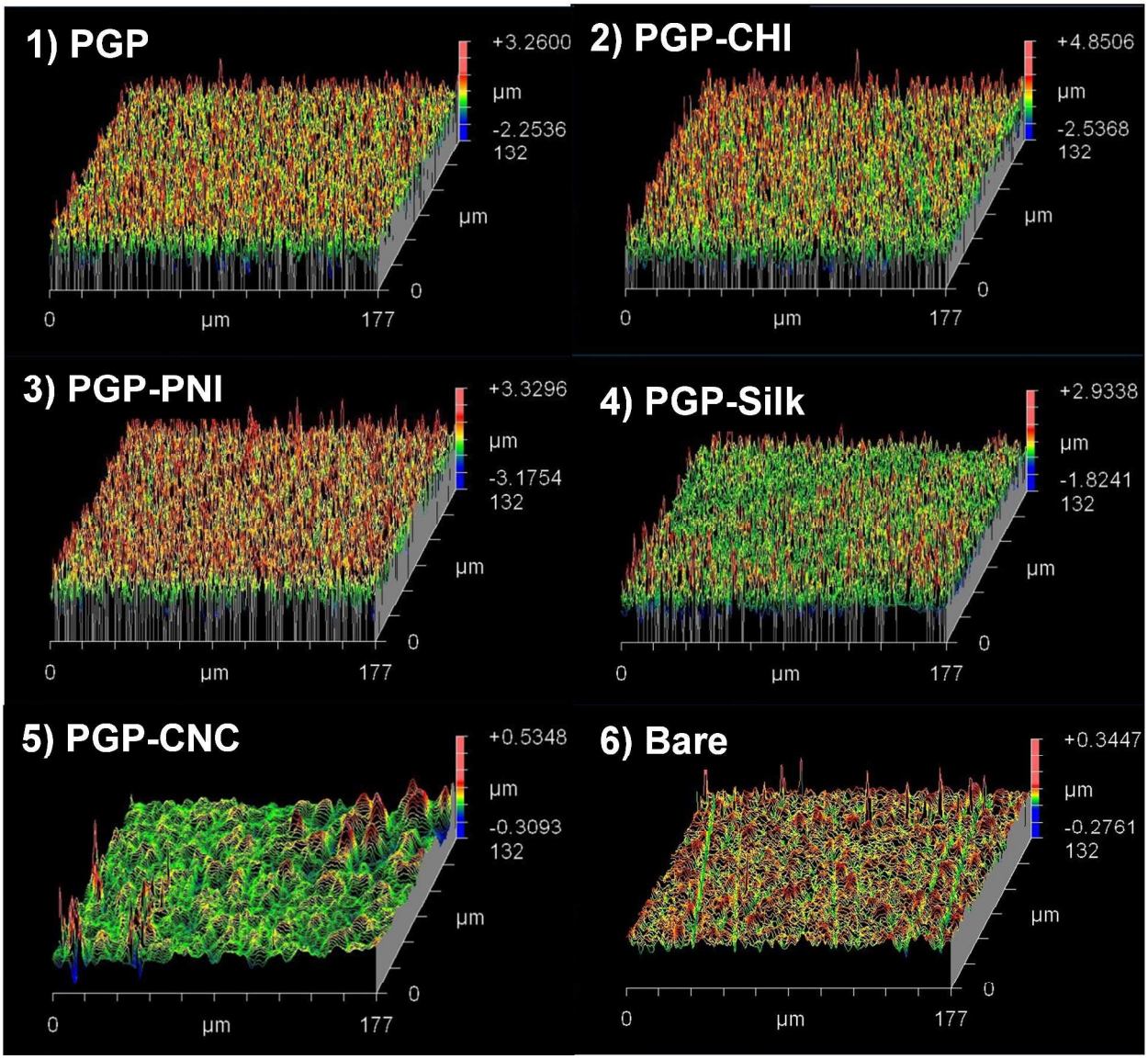

Figure S1. Representative SWLI images for all bionanocomposites. RMS values for each treatment were measured in triplicate (n > 3): 1=PGP (RMS = 587.0 ± 63.4 nm), 2=PGP_CHI (RMS = 699.5 ± 113.2 nm), 3=PGP_PNI (RMS = 712.6 ± 31.4 nm), 4=PGP_SILK (RMS = 267.9 ± 144.2 nm), 5=PGP_CNC (RMS = 44.8 ± 0.8 nm), 6=Bare (RMS = 25.89 ± 1.83 nm).

View Article Online
DOI: 10.1039/C4AN01788A

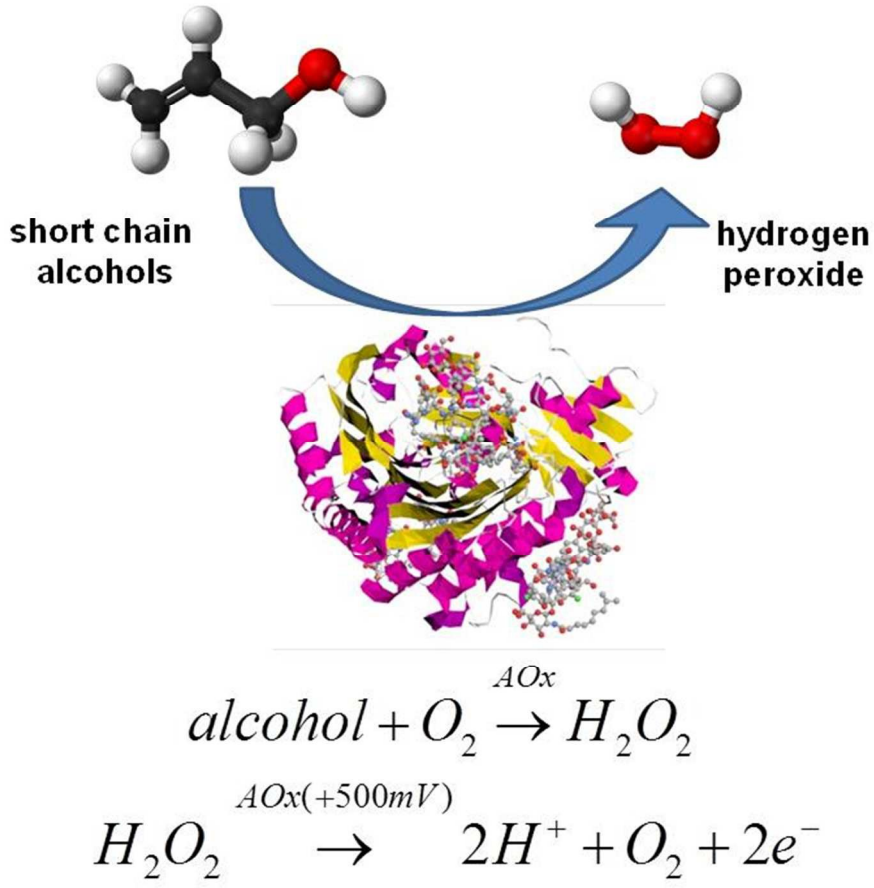

Figure S2. Schematic diagram depicting the oxidation of short chain alcohols by alcohol oxidase (AOx). Byproducts of this reaction are carbonyl compounds and hydrogen peroxide. Under oxidative bias, hydrogen peroxide deprotonates to produce free electrons which are measured as current (not drawn to scale).

View Article Online
DOI: 10.1039/C4AN01788A

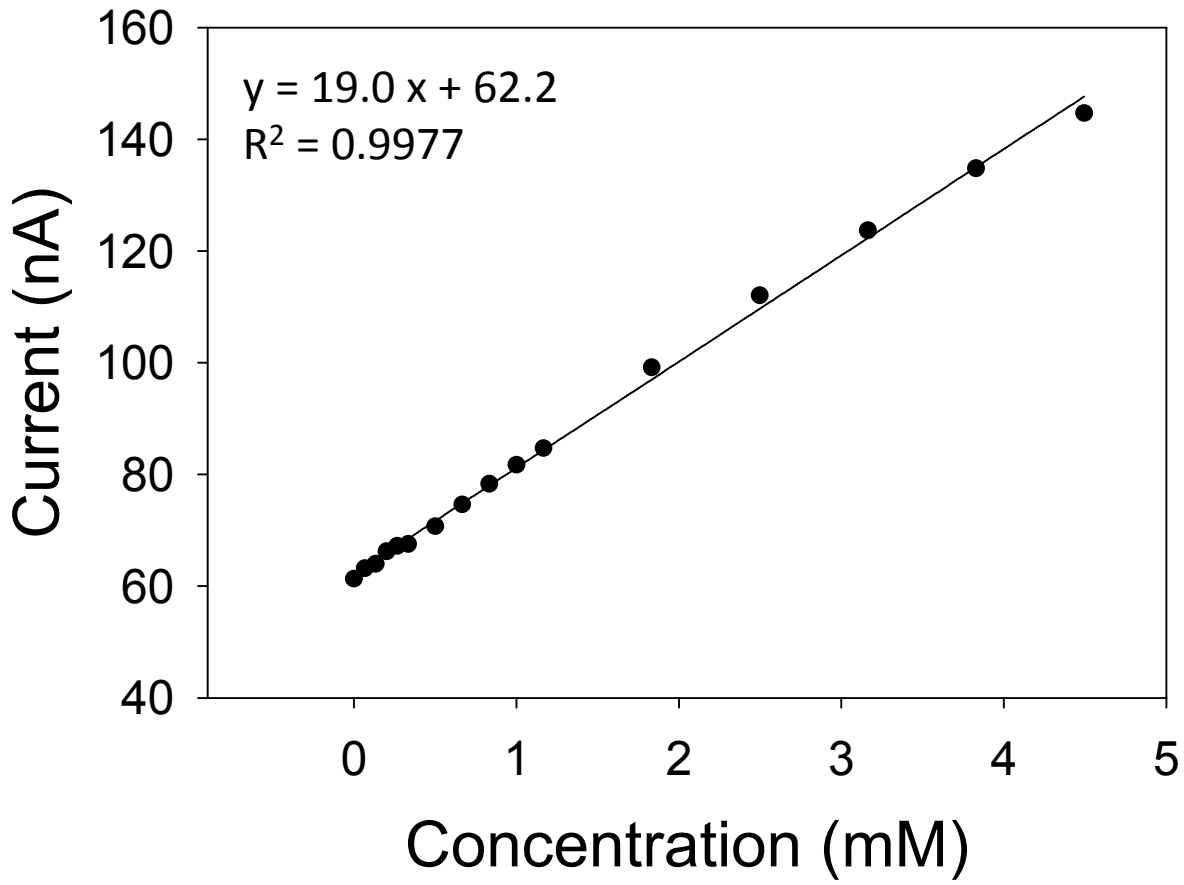

Figure S3. Representative average current versus methanol concentration plot from DCPA time series for AOx immobilized in chitosan on a PGP sandwich nanocomposite platform.

View Article Online
DOI: 10.1039/C4AN01788A

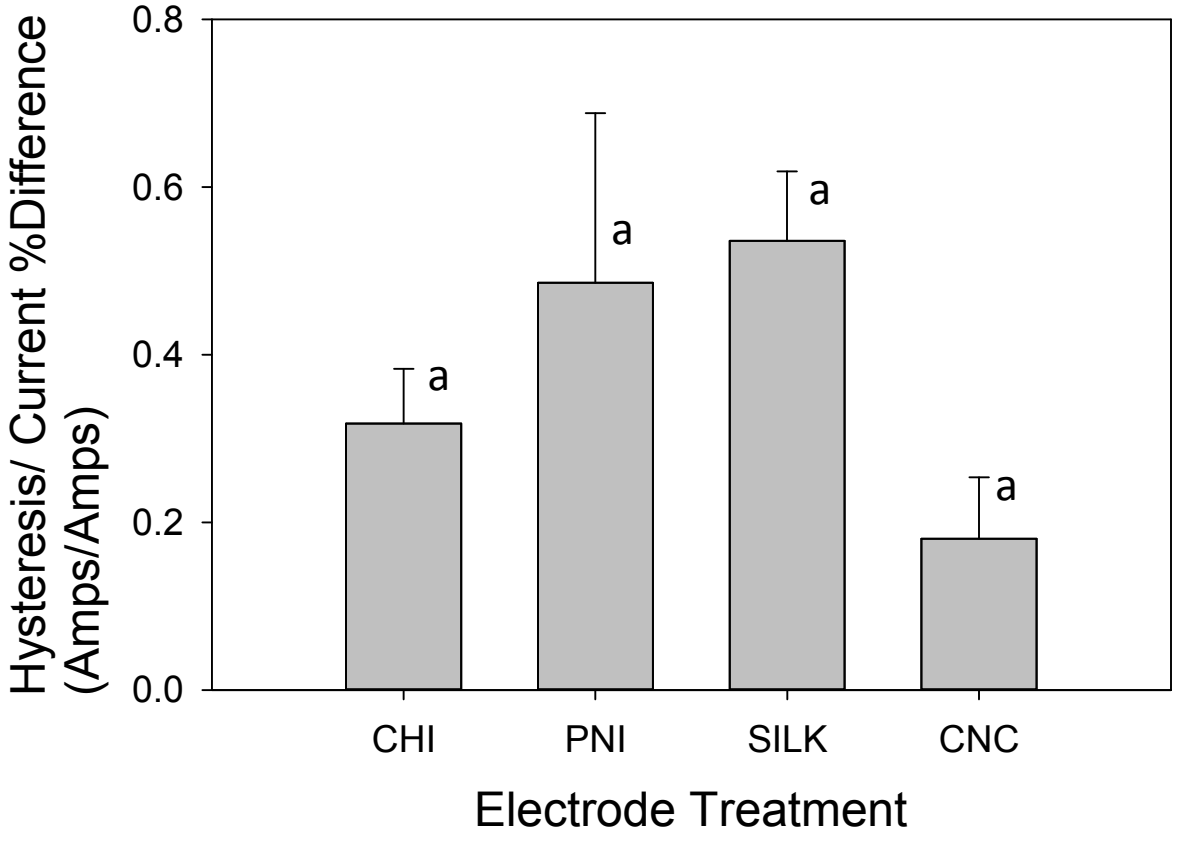

Figure S4. Average percent difference in polarization current for treated electrodes. Hysteresis measurements for AOx immobilized in various hydrogels on PGP-modified electrodes ($n \geq 3$). PGP_CHI= 31.8% ± 6.6%, PGP_PNI= 48.6% ± 20.2%, PGP_SILK=53.6% ± 8.3%, PGP_CNC=18.0% ± 7.3%. A Tukey pairwise comparison was used to group electrodes with no statistically significant differences in performance (indicated by the letter a).

View Article Online
DOI: 10.1039/C4AN01788A

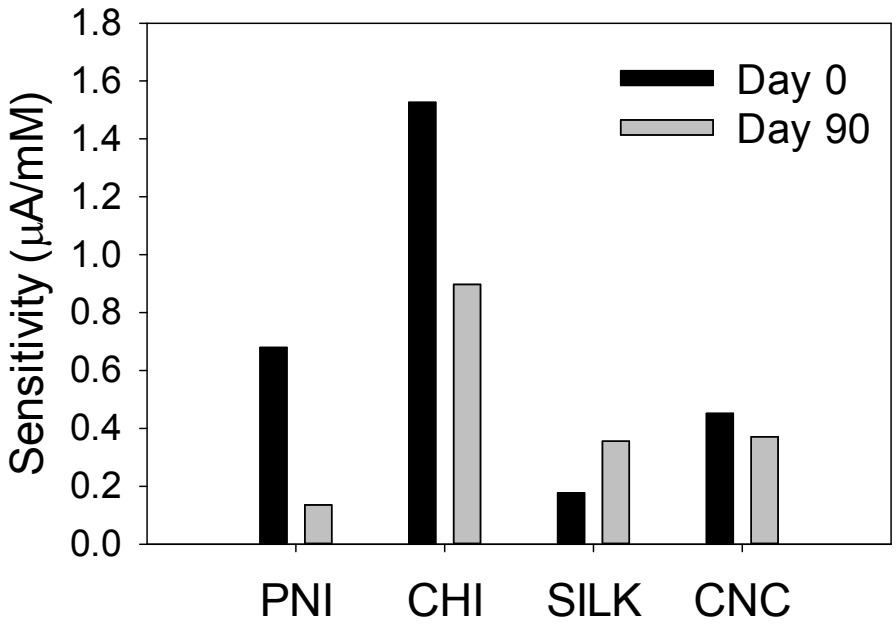

Figure S5. Shelf life study of hybrid bionanocomposites after storage in PBS at 4°C